SCIENTIFIC REPORTS
nature research

OPEN

Symmetry selected quantum dynamics of few electrons in nanopillar transistors

Yue-Min Wan* & Heng-Tien Lin

Study on single electron tunnel using current-voltage characteristics in nanopillar transistors at 298 K show that the mapping between the N_{th} electron excited in the central box $\sim 8.5 \times 8.5 \times 3\ nm^3$ and the N_{th} tunnel peak is not in the one-to-one correspondence to suggest that the total number N of electrons is not the best quantum number for characterizing the quality of single electron tunnel in a three-dimensional quantum box transistor. Instead, we find that the best number is the sub-quantum number n_z of the conduction z channel. When the number of electrons in n_z is charged to be even and the number of electrons excited in the n_x and n_y are also even at two, the adding of the third electron into the easy n_x/n_y channels creates a weak symmetry breaking in the parity conserved x-y plane to assist the indirect tunnel of electrons. A comprehensive model that incorporates the interactions of electron-electron, spin-spin, electron-phonon, and electron-hole is proposed to explain how the excited even electrons can be stabilized in the electric-field driving channel. Quantum selection rules with hierarchy for the n_i ($i = x, y, z$) and $N = \Sigma n_i$ are tabulated to prove the superiority of n_z over N.

Single electron tunnel (SET)[1] is an inspiring topic in quantum box transistors (QBTs)[2,3] owing to its diverse applications in single-electron devices such as digital memory cells, high precision electro-mechanical sensors and standardized meters[4,5] that consume one-tenth of pico-watt energy to upgrade the science and technology of semiconductors. With the application of a fixed, small bias on the drain-source electrodes and adjusting the bias on the gate electrode in a QBT, single electron tunnel peaks in current-voltage *(I–V)* characteristics can be manifested at a broad temperature range from milli Kelvin to 300 K. These peaks have been used to disclosure striking electro-quantum-mechanical effects which are known as Coulomb blockade[6], Coulomb-blockade oscillations[7,8], Coulomb staircases[9,10], single electron charging[11–13], zero-dimension states[14–16], competing channels[17], and two-level resonances[18–23] in various materials[24,25].

Theoretical understanding of these effects are based on two considerations. One relies on the classical charging energy $E_c = e^2/2C$ of multiple electrons in a parallel-plate capacitor that has been unanimously confirmed in constant peak spacings. The other depends on size quantization that appears to be more complicated because of the geometrical anisotropy in a three-dimensional (3D) QB. This property can lead to multiple charging energies E_n which will modulate peak's amplitudes[26] and spacings. Luckily enough, when the geometrical symmetry is introduced into the 3D QBT, the ordering of E_n can be brought out and reflects on the sub-quantum number n_i where *i* denotes the three independent variables x, y, z in a Cartesian coordinate; z, r, θ in a cylindrical coordinate and r, θ, ϕ in a spherical coordinate. Based on the circular symmetry in a two-dimensional (2D) electron gases, Tarucha *et al.* performed a study[27,28] on a disk QBT in zero magnetic field and found the one-to-one correspondence between the ionization energy of the N_{th} electron discharging from the N_{th} tunnel peak to uncover two magic quantum series. The first is all even numbers of 2, 6, and 12 claimed to be the full filling of electrons in the first, second, and third shells in a two-dimensional (2D) harmonic potential; the second is mixture of even and odd numbers at 4, 9, and 16 being claimed the half filling in the second, third and fourth shells to mimic three-dimensional (3D) spherically symmetric shells of 1*s*, 2*s*, 2*p*, 3*s*, 3*p*, etc. in real atoms to demonstrate the existence of artificial atoms.

These outstanding numbers no doubt prove the effectiveness of Pauli exclusion principle for spin-spin alignments between electrons and of Hund's rule for charge-charge interactions among electrons in different channels. However, the dynamical symmetry of n_i electrons are not explored, leading to the paucity of understanding how single electron tunnel is generated in the QBT. In our view, the N electrons will not be self-confined in the 2D x-y plane although they were assumed to be frozen at a very low temperature ~50 mK[26]. Some of the electrons ought to be excited and stabilized in the conduction channel and that will make the interactions between the electrons in

Department of Electronic Engineering, I-Shou University, Kaohsiung, Taiwan, ROC. *email: ymwan@cloud.isu.edu.tw

the x-y channels and those in the z channel critical which are believed to be the key of understanding the dynamical effects of SET in a deeper level; so does to the aforementioned seven effects.

In this paper, we will demonstrate such picture of n_i with the focus aiming on how the electrons excited in the narrow conduction z channel can be stabilized firstly, then on how they interact with the n_x and n_y electrons. It is found that the interactions of electron-electron, spin-spin, electron-phonon and electron-hole (exciton) in the z channel are vital in helping n_z becomes the most decisive quantum number. The electrons of n_x and n_y collaborate with the mechanical vibrations to assist the indirect tunnel of single electron. Each n_i is found to obey the fundamental rules of even number in doing electro-quantum mechanical stability and the odd number is in doing instability. As a harmony effect, the first peak generated in the stabilized SET is triggered by the addition of the third electron into the easy x and y channels when two (or four) electrons are pre-excited in the z channel. With all the n_i being assigned to all the peaks in the *I-V* spectrum, a comprehensive model is established to map out a full chart of n_i and N that eventually leads to the conclusion that n_z is the principle quantum number in characterizing the transport quality of single electron tunnel.

Mirror Symmetry of Moving Electrons in a Box

Once the importance of the dynamical symmetry is introduced[29], its influential effects must be established based on the degrees of balance and stability in a multiple electrons system by checking whether the moving electrons obey the symmetry of mirror images. When two electrons with antiparallel spins[30] and equally apart from the box's center move toward (or away from) each other in a one-dimensional well, the symmetry is called conserved; whereas when the condition is of one moving electron only, the symmetry has no chance to be conserved. Extending such an idea to 3D, the total N acting electrons and the sub acting n_i electrons in each channel clearly are periodical functions of the number 6 and 2, denoted as N_e and n_{ie}. At these numbers, the box is at the peak of stability. While at the middle odd numbers denoted as $N_o = 3$ and $n_{io} = 1$, the box is at the valley of stability. Assuming the N is increased at the steady pace of +1 for each tunnel peak, the N_e and n_{ie}, N_o and n_{i0} will alternatively play conservation and breaking of the global-3D and local-1D symmetries. In accordance, the N_e comes as the series of 0, 6, 12, 18…; the N_o as 3, 9, 15, 21…; the n_{ie} as 0, 2, 4, 6… and the n_{io} as 1, 3, 5, 7…etc. The combination of N_e and n_{ie} is possible and it becomes the series of 2, 8, 14, 20…; the $N_e + n_{io}$ of 1, 7, 13, 19…; the $N_o + n_{ie}$ of 5, 11, 17, 23… and the $N_o + n_{io}$ of 4, 10, 16, 22…etc. The combination of $n_{ie} + n_{io}$ no doubt will become the most flexible and popular states. These values will be confirmed later.

Transport measurements are performed on nanopillar transistors. The QB size in the devices is $\sim 8.5 \times 8.5 \times 3$ nm^3 that makes the lateral to normal length ratio 3 to 1, better than the disk QB of 8 to 1. The method adopted to analyze the $I_d - V_{ds}$ characteristics is unprecedented. Both the N and the n_i of each peak are determined. With these information, the total electronic numbers determined are up to $n_z = 4$ and $N = 28$. Given the sizes, Eq. (1) is used to calculate all the possible single-particle states, denoted as $[n_x, n_y, n_z]$, along with the associated energies E_n within 1 eV[31]. Table 1 summarizes all of them. Devices A and B were selected for discussions. Their qualities were checked by the as-fabricated *I-V* plots shown in the inset of Fig. 1. Both curves clearly exhibited symmetric effects of Coulomb blockades with $CV_{ds} = e$ at $V_{ds} \leq \pm 0.13$ V of $I_d = 0$ A. The value of C was determined to be ~ 1.2 aF which exactly matched the net value of the SiN_x-Si-SiN_x trinature frequency and-capacitors in demonstrating their high qualities.

$$E(n_x, n_y, n_z) = \frac{\pi^2 \hbar^2}{2m}\left(\frac{n_x^2}{L^2} + \frac{n_y^2}{W^2} + \frac{n_z^2}{H^2}\right) \tag{1}$$

Results and Discussions

Coulomb-blockade oscillations in nz = 0. As shown in Fig. 2(b), the first two electrons of the [1, 1, 0] state generate a moderate electron-phonon interaction by yielding Coulomb vibrations and subsequent currents. The alternating currents at $V_{ds} < 30$ mV suggest that the n_x and n_y electrons which are scattering created from the *Electric*-field in the z-channel. Their circular motions are dissipative and force free that can be described by the classical equation of motion with the induced current[32] as

$$I(t) = neA\alpha\omega e^{-\xi\omega_n t}\cos(\omega t + \varphi) \tag{2}$$

where n is silicon density, A box area, α maximum displacement, ξ damping ratio c/c_c, $c_c = 2\,m\omega_n$, $\omega = \omega_n(1-\xi^2)^{1/2}$, $\omega_n = (k/m)^{1/2}$ nature frequency and φ the initial phase. The good numerical fit to data in $t \leq 0.3$ s proves that the paired electrons are indeed doing harmonic motions and the phase φ is also determined to be $\pi/2$.

When the third electron is added to the QB for the state [1, 1, 1]. The dynamics of $n_z = 1$ electron show up. As illustrated in Fig. 3(a,b), the *E*-field generated free electron can lead to significant deformations and mechanical feedbacks in the QBT[33]. At the very first moment of a small bias being applied onto the box, as shown in Fig. 3(a), surface charges of positive and negative polarities will be built up on all interfaces[34], denoted as Q_s and q_s, respectively. When the eV_{ds} reaches $E(n_z = 1) \sim 42$ meV, the electron generates a large Coulomb force to bend the box into $\pm z$ directions sequentially as illustrated in Fig. 3(b). Note that the initial repulsive force is on the q_s^-, and it will then result in a forward current +I(t). The elasticity of the QB will restore it to its initial position, and excite the hole to provide a counterforce on the other end of the QB for a backward current −I(t). As results, zig-zag currents[35,36] are created between [1, 1, 0] and [1, 1, 1] states.

Unstable single electron tunnel in nz = 1, 3. At the state [3, 2, 1] of six electrons, the first SET shows up in Fig. 2(c) and it is triggered by the addition of the $n_x = n_y = 3$ electron into the [2, 2, 1] state (see Table 1). After that, the first series (#1) of SET develops as the N is increased from 6 to 9, [6, 2, 1], for a total of seven sharp peaks.

[n_x , n_y , n_z]	E_n(meV)	[n_x , n_y , n_z]	E_n(meV)	[n_x , n_y , n_z]	E_n(meV)	[n_x , n_y , n_z]	E_n(meV)
[1,0,0][0,1,0]	5.8	[4,2,2][2,4,2]	284.7	[6,4,2][4,6,2]	472.7	[6,4,3][4,6,3]	681.7
[1,1,0]	11.6	[6,3,1][3,6,1]	306.2	[4,1,3][1,4,3]	476.0	[7,2,3][2,7,3]	687.6
[0,0,1]	41.8	[4,3,2][3,4,2]	314.1	[7,5,1][5,7,1]	476.7	[2,1,4][1,2,4]	698.0
[1,1,1]	53.5	[5,1,2][1,5,2]	319.9	[7,2,2][2,7,2]	478.6	[2,2,4]	715.6
[2,1,1][1,2,1]	71.2	[7,1,1][1,7,1]	335.6	[3,3,3]	481.8	[7,3,3][3,7,3]	716.9
[2,2,1]	88.8	[5,5,1]	335.6	[4,2,3][2,4,3]	493.6	[3,1,4][1,3,4]	727.4
[3,1,1][1,3,1]	100.6	[5,2,2][2,5,2]	337.6	[7,3,2][3,7,2]	508.0	[6,5,3][5,6,3]	734.6
[3,2,1][2,3,1]	118.2	[6,4,1][4,6,1]	347.4	[4,3,3][3,4,3]	522.9	[7,7,2]	743.1
[4,1,1][1,4,1]	141.7	[7,2,1][2,7,1]	353.2	[6,5,2][5,6,2]	525.6	[3,2,4][2,3,4]	745.0
[3,3,1]	147.6	[4,4,2]	355.2	[5,1,3][1,5,3]	528.9	[7,4,3][4,7,3]	758.1
[4,2,1][2,4,1]	159.3	[5,3,2][3,5,2]	367.0	[7,6,1][6,7,1]	541.3	[4,1,4][1,4,4]	768.5
[1,1,2]	178.9	[7,3,1][3,7,1]	382.6	[5,2,3][2,5,3]	546.5	[3,3,4]	774.4
[4,3,1][3,4,1]	188.7	[6,1,2][1,6,2]	384.6	[7,4,2][4,7,2]	549.1	[4,2,4][2,4,4]	786.2
[5,1,1][1,5,1]	194.6	[1,1,3]	387.9	[4,4,3]	564.2	[6,6,3]	799.2
[2,1,2][1,2,2]	196.5	[6,5,1][5,6,1]	400.3	[5,3,3][3,5,3]	575.9	[7,5,3][5,7,3]	811.0
[5,2,1][2,5,1]	212.2	[6,2,2][2,6,2]	402.2	[6,6,2]	590.3	[4,3,4][3,4,4]	815.5
[2,2,2]	214.2	[2,1,3][1,2,3]	405.5	[6,1,3][1,6,3]	593.5	[5,1,4][1,5,4]	821.4
[3,1,2][1,3,2]	225.9	[5,4,2][4,5,2]	408.1	[7,5,2][5,7,2]	602.0	[5,2,4][2,5,4]	839.0
[4,4,1]	229.8	[2,2,3]	423.1	[6,2,3][2,6,3]	611.2	[4,4,4]	856.7
[5,3,1][3,5,1]	241.6	[7,4,1][4,7,1]	423.8	[5,4,3][4,5,3]	617.0	[5,3,4][3,5,4]	868.4
[3,2,2][2,3,2]	243.6	[6,3,2][3,6,2]	431.6	[7,7,1]	617.7	[7,6,3][6,7,3]	875.6
[6,1,1][1,6,1]	259.2	[3,1,3][1,3,3]	434.9	[6,3,3][3,6,3]	640.5	[6,1,4][1,6,4]	886.1
[4,1,2][1,4,2]	267.1	[3,2,3][2,3,3]	452.5	[7,6,2][6,7,2]	666.7	[6,2,4][2,6,4]	903.7
[3,3,2]	272.9	[7,1,2][1,7,2]	461.0	[7,1,3][1,7,3]	669.9	[5,4,4][4,5,4]	909.6
[6,2,1][2,6,1]	276.9	[5,5,2]	461.0	[5,5,3]	669.9	[6,3,4][3,6,4]	933.1
[5,4,1][4,5,1]	282.7	[6,6,1]	464.9	[1,1,4]	680.4		

Table 1. Three-dimensional quantized states and energies of a $8 \times 8 \times 3\,nm^3$ box. The data are calculated from Eq. (1) (see main text). The states in magenta, dark cyan, red, blue and orange colors correspond to those of $n_z = 0, 1, 2, 3$ and 4. It is evident that in the highly symmetric device B, the number of states selected is very few ~13, while in the less symmetric device A, the states selected are vast, more than 40.

Each peak is clean in singlet state, suggesting a unique vibration mode is involved, and they are separated by a seemingly constant distance. For the QB of A ≈ $8.5 \times 8.5\,nm^2$ and H = 3 nm, the $E_c = e^2/2C$, $C = \varepsilon_r\varepsilon_o A/D \sim 3.5$ aF, $\varepsilon_r = 11.7$, $\varepsilon_o = 8.85 \times 10^{-12}\,C^2/Nm^2$ is estimated to be ~30 meV. This value is expected to match the peak spacing ΔE_n well and as matter of fact, in Fig. 4(a), the ΔE_n varies strongly from peak to peak with the 1st ~30 meV and the 6th ~18 meV that yields a statistical value ~24 ± 6 meV and a mean deviation over 20%. The large deviation indicates that the $n_z = 1$ SET of is not stable, with spin 1/2. As a consequence, the SET stops at the states [4, 2, 2]/[2, 4, 2] and [4, 4, 2] of $n_z = 2$ which have s = 0.

Notably, at a higher eV_{ds} ~0.4 eV, the stopped SET revives itself by changing from the singlet to doublet state (meaning L ≠ W), and also by regrouping the n_i to increase the n_z from 1 to 3 while maintaining the total N fixed at 6. In the following 10 split peaks, the N quickly increases from 12 to 24. Thanks to the extra stability introduced by the doublet states[17], the #2 SET runs a little bit longer than the #1. Accordingly, the distributions of ΔE_n becomes a uniform value of ~25 ± 3 meV in Fig. 4(a). Nevertheless, these peaks still show progressively decays in amplitudes for another end near 0.7 V to prove that the odd $n_z = 3$ is still unstable (s = 1/2).

Stable single electron tunnel in nz = 2, 4. To make the $n_z = 2$ SET happen, device B is used. In Fig. 5(a), it is again that giant Coulomb currents dominate the I_d–V_{ds} from 0 to −0.23 V. The first peak emerges right at the doublet [3, 2, 2]/[2, 3, 2] states to confirm that the starting n_z is indeed 2[14]. After that the SET peaks are well spaced by a ΔE_n which is estimated to be ~33 ± 3 meV. This value matches the E_c ≈34 meV very well. By checking with Table 1, the ground state of all the two-level resonances is at the most balanced $N_e = 6$, [2, 2, 2] state. The gap

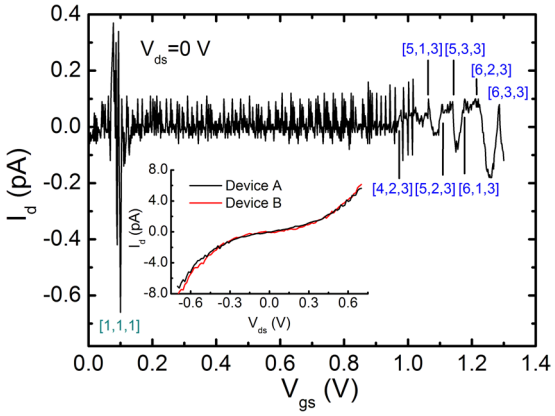

Figure 1. I_d versus V_{gs} of device B at 298 K. Giant Coulomb currents are clear near 0.1 V. The leading 3D electronic states of $n_z = 3$ dominate the tunnel peaks at high bias. Inset shows Coulomb blockades of device A and B as fabricated.

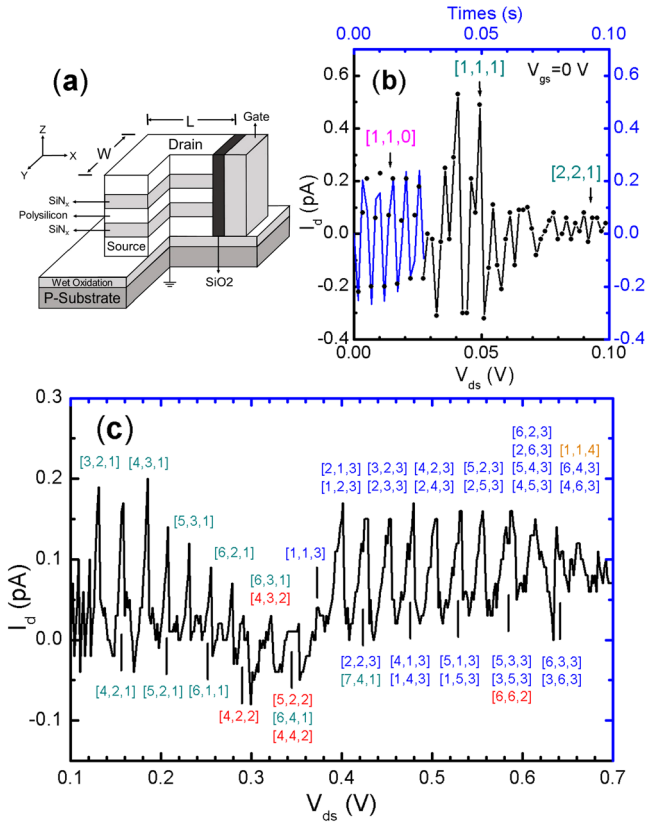

Figure 2. Device structure and current-voltage characteristics of device A at 298 K. **(a)** A schematic view of nanopillar transistor. **(b)** A theoretical fit and data. The blue curve is the damping current calculated from Eq. (2) (see main text). Parameters used in the fit are $n = 5 \times 10^{22}/cm^3$, $A = 72\ nm^2$, $\alpha = 3$ Å, $\omega = 1.16 \times 10^3$ Hz, $\varphi = \pi/2$ and $\xi = 6 \times 10^{-3}$. **(c)** I_d–V_{ds} at large bias. The 3D electronic states of each tunnel peak are labeled in brackets, referring to Table 1. Odd peaks are labeled on top and even peaks are below. The first series of single-electron tunnel at $n_z = 1$ is in dark cyan, the second series of $n_z = 3$ is in blue. The states at $n_z = 2$ and 4 of stop zones are in red and orange.

$\Delta E_n \sim 29.4$ meV between [2, 2, 2] and [3, 2, 2]/[2, 3, 3] is an excellent value near E_c. No wonder that the stable SET runs very long for a total of 21 doublet peaks[24]. In fact, they are triggered by the $N = N_e + n_{io} = 6 + 1 = 7$ electron in each mode with $2N = 14$ in total. *In another words, it is the third electron added to the stable $n_x = n_y = 2$ states creating the weak dynamical break to assist one electron tunnel in the z-channel.* Inset of Fig. 5(b) illustrates how this $n_x/n_y = 3$ electron can take advantage of the two-level vibrations[18–23]; it is firstly charged into the n_x/n_y channels, then propelled out of them into the main channel for a current peak.

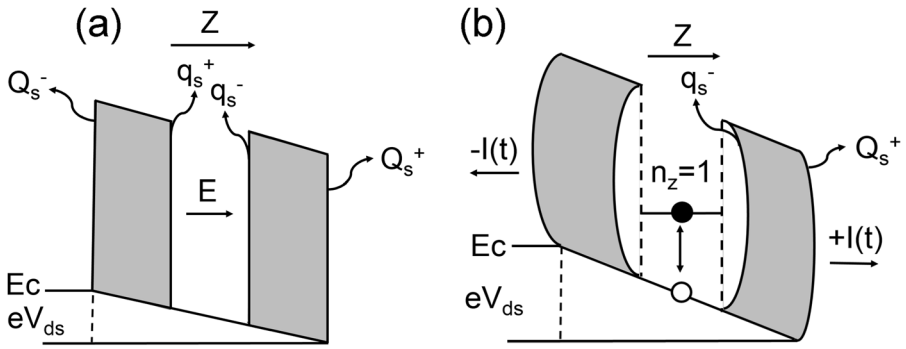

Figure 3. Dielectric response under the action of a drain-source voltage. (**a**) An electric field *E* is initiated inside of the box with accumulated surface charges Q_s^-, q_s^+, q_s^- and Q_s^+. (**b**) Single electron excited to state $n_z = 1$ and box deformations. A hole is also created. Coulomb forces between electron and q_s^- and q_s^+ generate forward +I(t) and backward −I(t) currents.

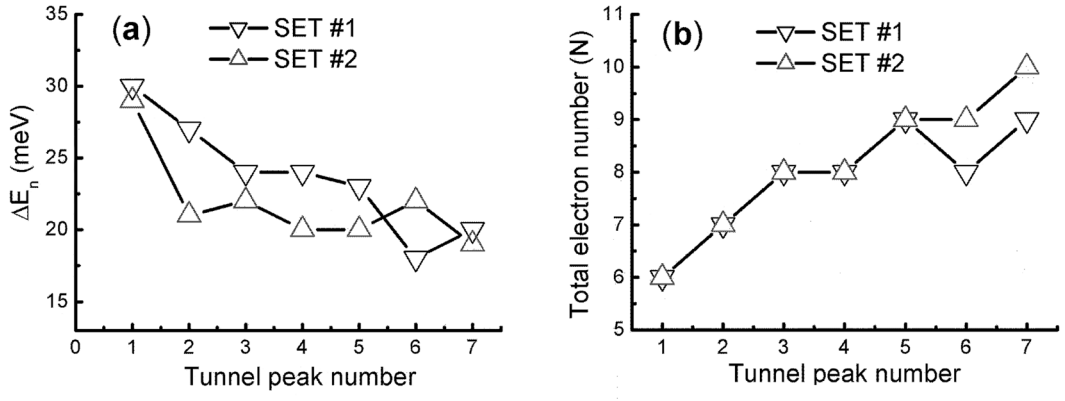

Figure 4. Single electron tunnel peak dependence of charging energy and total electron number N. (**a**) Peak number versus charging energy. The first point represents the energy gap between [2, 2, 1] and [3, 2, 1] states. The remaining points represent the energy spacing between two neighboring peaks in Fig. 2(c). (**b**) Peak number versus N. The instability of N is clear as it comes across the number of 9.

At $eV_{ds} \sim -0.92$ eV, the SET makes a transition to double electron tunnel (DET) by presenting a sharp increase in the magnitude of I_d that resembles the Coulomb staircases which have been spotted elsewhere[9,10]. The cause of this transition is created by the same $\Delta E_n \sim 29.4$ meV which is amazing. Notice that although the DET occurs at the next even $n_z = 4$, the same $n_x/n_y = 2 \leftrightarrow 3$ resonance remains active. Ideally, the resonance should happen at the global ground state of [4, 4, 4] (just like [2, 2, 2]) and then jump to the higher states of [5, 4, 4]/[4, 5, 4], but that would require an much higher energy ~53 meV which is almost impossible. As an alternation, the QBT skips three energy levels until the meet of the doublet ground states [6, 2, 4]/[2, 6, 4]; therein the QBT makes the transition to the doublet [6, 3, 4]/[3, 6, 4] states. As a reward, one more conduction channel is created, as shown in the inset of Fig. 5(a), making electrical conduction more efficient. In the meantime, the total N reaches the highest value of $4N_e + 4n_o = 28$.

The robust SET and DET are reproducible from a high bias. In Fig. 5(b), when the bias begins with the −1 V, the DET shows no sign of fading at all in the beginning. The EQM coherence remains firmly locked with the $N = 24 \leftrightarrow 28$ transitions, with the only difference being the φ shifted from the $\pi/2$ ($t = 0$ s) to π. At the all even [4, 4, 4] state, the DET makes a decay to the SET. After that, the $N = 12 \leftrightarrow 14$ resonances take over and run the SET all of the way to $V_{ds} = 0$ V to convince the initial Coulomb-blockade oscillations observed in Fig. 2(b). These data also explain the long-time search of why the classical E_c is an excellent indication of stable electron charging energy and it is only when the E_n matches its value, the coherent SET will show up. Other than the outstanding finding, the breakdown of the one-to-one correspondence between the N and the tunnel peaks is also remarkable as it indicates that there will have multiple peaks in corresponding to the same electron numbers and their effects will be discussed in the following paragraph.

Excitation of holes to neutralize electrons. The transition from DET to SET drastically changes the value of N. Here, the ΔN is as large as 16, from 28 to 12 at the state of [4, 4, 4] that makes 16 excited electrons left over to be annihilated by holes[37]. As results of the holes excitations illustrated in Fig. 3(b), negative mechanical

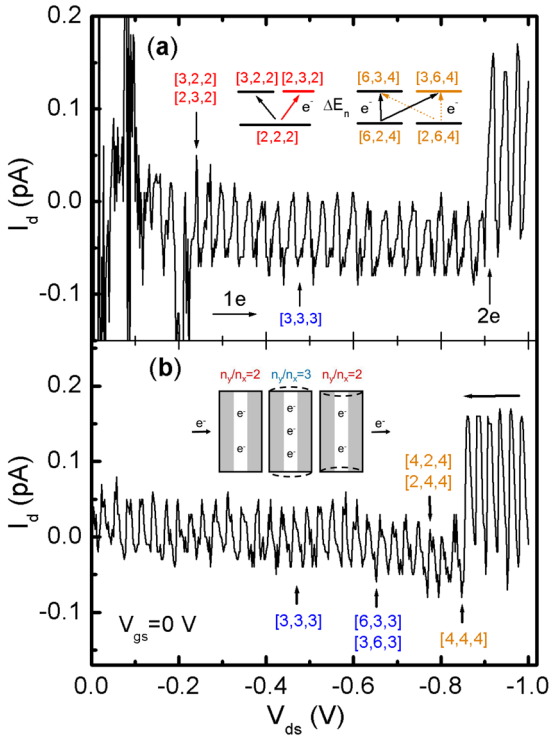

Figure 5. I_d versus V_{ds} of device B at 298 K. Note that the polarity of current is changed. (**a**) Electron charging from 0 to 1 V. The first peak is at [3, 2, 2]/[2, 3, 2] doublet. Double electron tunnel begins at [6, 2, 4]/[2, 6, 4] states. Inset (left) shows two-level resonance of one electron tunnel; (right) two-channel, two-level resonance tunnels of double electrons. (**b**) Reversed charging from −1 to 0 V. Transition from 2*e* to 1*e* tunnel is at [4, 4, 4] state. Inset shows the vibration assisted electron tunnel; from left to right, prior to the entrance of 1*e*, resonances with 2*e* in the n_y/n_x channels, and repel of the charged electron.

feedbacks will constantly act on the drain electrode for negative currents to lower the level of I_d. As a consequence, after the largest drop at [4, 4, 4], the next drop develops at the doublet [4, 2, 4]/[2, 4, 4], then is the hidden $n_z = 3$ [6, 3, 3]/[3, 6, 3] doublet states, following by the all odd singlet [3, 3, 3] right in the middle of the SET series. Notably, in Fig. 5(a) of electron charging in device A, the [3, 3, 3] state is also becoming visible in a dip to signal that the weakly bonded pairs of electrons and holes (excitons) are important dynamical entities. The same effect is also detected in Fig. 2(c), when the ΔN is not increased in pace with the $+\Delta eV_{ds}$, three drops appear at the [4, 2, 2], [4, 3, 2]/[3, 4, 2], [4, 4, 2] and [5, 2, 2]/[2, 5, 2] states.

Interferences in two conduction channels. Electron charging from the side gate confirms the high flexibility of $n_{ie} + n_{io}$. Here the n_{ie} represents the sum of n_{xye} and n_{xyo}, and the n_{io} is the n_{zo}. The reason is simple because the driving *E*-field will be separated into two components; one is along the side channel and the other is along the main channel. As results of their interference acting[38], the states excited are most likely to be the highest probability but with the lowest symmetry. As shown in Fig. 1, The first giant currents of [1, 1, 1] again appear at $V_{gs} \sim 0.1$ V. When compared to the noise at 50 mV in Fig. 2(b), the gate-dot coupling strength is determined to be 0.5. Based on this value, the successive leading peaks for SET are identified to be the following states; [4, 2, 3], [5, 1, 3], [5, 2, 3], [5, 3, 3], [6, 1, 3], [6, 2, 3] and [6, 3, 3]. Notice that there are no all even states like N_e, the starting N_o is at 3, then is the isotropic state of $N_o = 9$, [4, 2, 3], the N then fluctuates down and up in the states of $n_z = 3$. At the [6, 3, 3], an isotropic state of $N = 12$, a sharp peak appears in reminding of the end in SET #2.

Quantum selection rules in 3D box transistors. As listed in Table 2, the hierarchy of symmetry in terms of the N_e, N_o, n_{ie}, and n_{io} becomes very clear and the result is $N_e > n_{ie} > n_{io} > N_o$. N_o of the lowest stability manifests itself as the giant Coulomb currents in [1, 1, 1] and [3, 3, 3]. The [1, 1, 1] state also serves to activate the QBT for later on tunneling of electrons. In sharp contrast, the N_e provides the highest stability in [2, 2, 2] and [4, 4, 4] states for an activated QBT. The primary combination of $N_e + n_{xyo}$ then creates the most needed tunneling of single electron. The secondary combination of $n_{ie} + n_{xyo}$ generates the most urgently needed two-channel, two-level resonance tunneling of double electrons. In between, the combination of $n_{xye} + n_{xyo} + n_{zo}$ creates most of the unstable SET and they will be temporarily stopped at the states of $n_{xye} + n_{xyo} + n_{oe}$. According to these rules, the previously claimed *not-all* odd magic number of 4, 9, and 16 in disk QBT could be either the all odds number of 3, 9, 15, or the composition of $n_{xye} + n_z$ with the latter being the incremental number of 0, 1, and 2. After subtracting the n_z, that leaves the $n_{xye} = 4$, 8, and 14 which fit perfectly into the *claimed* all even numbers of 2, 6, and 12.

	Device A								Device A						
	$[n_x, n_y, n_z]$	n_z	N	N_e	n_{ie}	n_{io}	N_o		$[n_x, n_y, n_z]$	n_z	N	N_e	n_{ie}	n_{io}	N_o
Charging $n_z = 0, 1$	[1, 1, 0]	0	2		O	O		$n_z = 3, 4$	**[4, 1, 3]**	3	16		O	O	
	[1, 1, 1]	1	3			O			**[4, 2, 3]**	3	18		O	O	
	[2, 2, 1]	1	5		O	O			**[5, 1, 3]**	3	18			O	
	[3, 2, 1]	1	6		O	O			**[5, 2, 3]**	3	20		O	O	
	[4, 2, 1]	1	7		O	O			**[5, 3, 3]**	3	22			O	
	[4, 3, 1]	1	8		O	O			**[6, 2, 3]**	3	22		O	O	
	[5, 2, 1]	1	8		O	O			**[5, 4, 3]**	3	24		O	O	
	[5, 3, 1]	1	9			O			**[6, 3, 3]**	3	24		O	O	
	[6, 1, 1]	1	8		O	O			**[6, 4, 3]**	3	28		O	O	
	[6, 2, 1]	1	9		O	O			[1, 1, 4]	4	6		O	O	
	[6, 3, 1]	1	10		O	O			**Device B**						
	[6, 4, 1]	1	11		O	O			$[n_x, n_y, n_z]$	n_z	N	N_e	n_{ie}	n_{io}	N_o
	[7, 4, 1]	1	12		O	O		Charging	[2, 2, 2]	2	6	O	O		
$n_z = 2, 3$	[4, 2, 2]	2	8		O				**[3, 2, 2]**	2	14		O	O	
	[4, 3, 2]	2	9		O	O			[3, 3, 3]	3	9			O	O
	[5, 2, 2]	2	9		O	O			**[6, 2, 4]**	4	24		O		
	[4, 4, 2]	2	10		O				**[6, 3, 4]**	4	28		O	O	
	[6, 6, 2]	2	14		O			Discharging	**[6, 3, 4]**	4	28		O	O	
	[1, 1, 3]	3	5			O			[4, 4, 4]	4	12	O	O		
	[2, 1, 3]	3	12		O	O			**[4, 2, 4]**	4	20		O		
	[2, 2, 3]	3	7		O	O			**[6, 3, 3]**	3	24		O	O	
	[3, 2, 3]	3	16		O	O			[3, 3, 3]	3	9			O	O

Table 2. Three-dimensional electronic states identified in device A and B. Hierarchy of quantum numbers denoted and classified by N_e, n_{ie}, and n_{io} and N_o symbols. N_e has the highest symmetry in a state with all even n_i and $n_x = n_y = n_z$. n_{ie} comes as the next with at least one even n_i in a state, n_{io} is ranked as the third with at least one odd n_i in a state. N_o is the lowest in ranking with all odd n_i and $n_x = n_y = n_z$ in a state. Bold state means doublet states. It is clear that the increment of n_z in charging is much steadier than N.

Vibrational frequencies and maximum displacements. Vibrational frequencies induced by the electron-phonon interactions in the QBTs are estimable. The most outstanding one clearly is the [1, 1, 1] as plotted in Fig. 2(a). Its ν_z is fitted to be $\sim 1.85 \times 10^2$ Hz and the maximum displacement of α_z is fitted to be ~ 3 Å. At $N = 7$, the values of ν_y and ν_x are expected to be higher, ~ 100 times larger than the initial frequency. Since the C of the two devices is approximate ~ 3.5 aF and the R is $\sim 2 \times 10^{13}$ Ω that leads the RC $\sim 4.4 \times 10^{-5}$ s and the ν_x/ν_y $\sim 2.2 \times 10^4$ Hz. By taking this value into $I_d = e\nu_y$, a peak current of 0.15 pA is obtained, which agrees with the data very well. With the vibrating frequency being increased at the $n_z = 3$ states, the α_y or α_x will become smaller. For an isotropic electron mobility in the QB, the I_d equals $neA\upsilon_d$ with $\upsilon_d = \alpha\omega_y/2\pi$. Given the $n = 10^{19}/cm^3$ and $A = 64$ nm^2, the α_y (or α_x) is calculated to be ~1 Å.

In conclusion, we study the dynamics of electrons in three-dimensional quantum box, nanopillar transistors. Single electron tunnel N_{th} peak is found not in one-to-one correspondence with the excited N_{th} electron. The best quantum number to describe SET is the sub-quantum number n_z in the conduction z channel, not the conventionally used total electron number N. Stable SET peaks occur only when the number of electrons excited in n_z is even and the number of electrons excited in the normal n_x/n_y channels are also even at two, robust peaks are then generated one-after-one by the charging/discharging of the third electron in/out of the normal x-y channels. A comprehensive model that incorporates the dynamical interactions of electron-electron, spin-spin, electron-phonon, and electron-hole explains the mechanical stability of even electrons in the electric-field driving z channel. Quantum selection rules with hierarchy of n_i and N are tabulated to prove that n_z is a better number than the N for characterizing the quality of electron tunnel.

Methods

Device fabrication and current-voltage measurements. The nanopillar transistor as shown in Fig. 2(a) was fabricated on a p-type (100) silicon wafer which featured a central polysilicon layer separated from the top and bottom electrodes by a nitride layer[39]. This center box had a critical thickness of 3 nm and was coupled to a side gate. Deposition of SiN_x (3-nm)-polysilicon (3-nm)-SiN_x (3-nm) layers were processed using a low-pressure chemical vapor technique, and then chemically etched it to create a nominal plateau $\sim 200 \times 140 \times 210$ nm^3. Phosphorous of a concentration 1×10^{19} cm^{-3} was doped in Si layer. The source was located at the bottom with a sheet resistance of ~30 Ω/cm^2. To prevent electrical shortage, a short oxidation was carried out to seal the nanopillar (creating another ~1.5 nm oxide). To further squeeze the cavity, the technique of self-aligned oxidation was utilized to add another ~6 nm layer of gate oxide, yielding a total of ~9 nm with the inner box reduced to the size $\sim 9 \times 9 \times 3$ nm^3. Finally, an Al (300 nm) side gate was attached. Devices were loaded into a probe station for *I-V* measurements at 298 K and a three-terminal HP meter with resolutions of 1 mV and 10 fA was used.

Zero magnetic field. To elucidate the authentic electron charging effects, external perturbations were kept to a minimum. No extra magnetic field was applied, except the negligible *Earth B*-field. Electrical bias was only applied either from the drain-source electrodes or the gate-source electrodes to avoid mutual interference in most cases.

Reduced sizes in parabolic potential. To count for the mutual interactions between multiple electrons in a parabolic potential, the values of L and W are reduced ∼5% smaller than the real values as the effectively electron-electron repulsions will make the QB smaller for a higher charging energy to the entrance of next electron. With these fine tunings, excellent agreements are reached between analysis and data.

Received: 2 September 2019; Accepted: 28 November 2019;
Published online: 27 December 2019

References

1. Grabert, H & Devoret, M. H. *Single Charge Tunneling* (Plenum Press, New York and London, 1992).
2. Kastner, M. A. Artificial atoms. *Phys. Today* **46**, 24 (1993).
3. Ashoori, R. C. Electrons in artificial atoms. *Nature* **379**, 413 (1996).
4. Likharev, K. K. Single-Electron Devices and Their Applications. *Proc. IEEE* **87**, 606 (1999).
5. Alferov, Z. I. The double heterostructure concept and its applications in physics, electronics, and technology. *Rev. Mod. Phys.* **73**, 767 (2001).
6. Averin, D. V. & Likharev, K. K. Coulomb blockade of single electron tunneling and coherent oscillation in small tunnel junction. *J. Low Temp. Phys.* **62**, 345 (1986).
7. Beenakker, C. W. J. Theory of Coulomb-blockade oscillations in the conductance of a quantum dot. *Phys. Rev. B* **44**, 1646 (1991).
8. Scott-Thomas, J. H. F., Field, S. B., Kastner, M. A., Smith, H. L. & Antoniadis, D. A. Conductance oscillations periodic in the density of a one-dimensional electron gas. *Phys. Rev. Lett.* **62**, 583 (1989).
9. Averin, D. V. & Korotkov, A. N. Influence of discrete energy spectrum on correlated single-electron tunneling via a mesoscopically small metal granule. *Sov. Phys. JETP* **70**, 937 (1990).
10. Su, B., Goldman, V. J. & Cunningham, J. E. Observation of single-electron charging in double-barrier heterostructures. *Science* **255**, 313 (1992).
11. Fulton, T. A. & Dolan, G. J. Observation of single-electron charging effects in small tunnel junctions. *Phys. Rev. Lett.* **59**, 109 (1987).
12. Meirav, U., Kastner, M. A. & Wind, S. J. Single-electron charging and periodic conductance resonances in GaAs nanostructures. *Phys. Rev. Lett.* **65**, 771 (1990).
13. Meurer, B., Heitmann, D. & Ploog, K. Single-electron charging of quantum-dot atoms. *Phys. Rev. Lett.* **68**, 1371 (1992).
14. Reed, M. A. *et al*. Observation of discrete electronic states in a zero-dimensional semiconductor nanostructure. *Phys. Rev. Lett.* **60**, 535 (1988).
15. Johnson, A. T. *et al*. Zero-dimensional states and single electron charging in quantum dots. *Phys. Rev. Lett.* **69**, 1592 (1992).
16. Ashoori, R. C. *et al*. Single-electron capacitance spectroscopy of discrete quantum levels. *Phys. Rev. Lett.* **68**, 3088 (1992).
17. Wies, J., Haug, R. J., Klitzing, K. V. & Ploog, K. Competing channels in single-electron tunneling through a quantum dot. *Phys. Rev. Lett.* **71**, 4018 (1993).
18. Gueret, P., Blanc, N., Germann, R. & Rothuizen, H. C Confinement and single-electron tunneling in Schottky-gated, laterally squeezed double barrier quantum well heterostructures. *Phys. Rev. Lett.* **68**, 1896 (1992).
19. Tewordt, M. *et al*. Single-electron tunneling and Coulomb charging effects in asymmetric double-barrier resonant-tunneling diodes. *Phys. Rev. B* **45**, 14407 (1992).
20. Chang, L. L., Esaki, L. & Tsu, R. Resonant tunneling in semiconductor double barriers. *Appl. Phys. Lett.* **24**, 593 (1974).
21. Dellow, M. W. *et al*. Resonant tunneling through the bound states of a single donor atom in a quantum well. *Phys. Rev. Lett.* **68**, 1754 (1992).
22. van der Vaart, N. C. *et al*. Resonant tunneling through two discrete energy states. *Phys. Rev. Lett.* **74**, 4702 (1995).
23. Bryant, G. W. Resonant tunneling in zero-dimensional nanostructures. *Phys. Rev. B* **39**, 3145 (1989).
24. Bitton, O., Gutman, D. B., Berkovits, R. & Frydman, A. Multiple periodicity in a nanoparticle-based single-electron transistor. *Nature Comm.* **8**, 402 (2017).
25. Chandrasekhar, V., Ovadyahu, Z. & Webb, R. A. Single-electron charging effects in insulating wires. *Phys. Rev. Lett.* **67**, 2862 (1991).
26. Reimann, S. M. & Manninen, M. Electronic structure of quantum dots. *Rev. Mod. Phys.* **74**, 1283 (2002).
27. Tarucha, S., Austing, D. G., Honda, T., van der Hage, R. J. & Kouwenhoven, L. P. Shell filling and spin effects in a few electron quantum dot. *Phys. Rev. Lett.* **77**, 3613 (1996).
28. Kouwenhoven, L. P. *et al*. Excitation spectra of circular, few-electron quantum dots. *Science* **278**, 1788 (1997).
29. Lee, T. D. & Yang, C. N. Question of parity conservation in weak Interactions. *Phys. Rev.* **104**, 254 (1956).
30. Hanson, R., Kouwenhoven, L. P., Petta, J. R., Tarucha, S. & Vandersypen, L. M. K. Spins in few-electon quantum dots. *Rev. Mod. Phys.* **79**, 1217 (2007).
31. Beiser, A. *Concepts of Modern Physics*, sixth edition (McGraw-Hill, New York, 2003).
32. Wang, T. C. & Wan, Y. M. Study of electron charging by voltage pulses in nanopillar transistors at high temperature. *Chin. J. Phys.* **55**, 1225 (2017).
33. Nishiguchi, N. Elastic deformation blockade in a single-electron transistor. *Phys. Rev. B* **68**, 121305 (1989).
34. Powell, M. J. Charge trapping instabilities in amorphous silicon-silicon nitride thin-film transistors. *Appl. Phys. Lett.* **43**, 597 (1983).
35. Nord, T., Gorelik, L. Y., Shekhter, R. I. & Jonson, M. Electromechanics of charge shuttling in dissipative nanostructure. *Phys. Rev. B* **65**, 165312 (2002).
36. Novotny, T., Donarini, A., Flindt, C. & Hauho, A.-P. Shot noise of a quantum shuttle. *Phys. Rev. Lett.* **92**, 248302 (2004).
37. Knox, R. S. *Theory of Excitons, Solid State Physics* (Ed. by Seitz and Turnbul, Academic, NY, v. 5, 1963).
38. Alhassid, Y. The statistical theory of quantum dots. *Rev. Mod. Phys.* **72**, 895 (2000).
39. Wan, Y. M., Lin, H. T., Sung, C. L. & Hu, S. F. Nanopillar transistors exhibiting single-electron quantum effects at room temperature. *Appl. Phys. Lett.* **87**, 123506 (2005).

Acknowledgements

We thank Taiwan Semiconductor Research Institute (TSRI) for device fabrication, and Jing Kai Lim, Han Loong Lee and Xin Xian Lin for essential assistance. This work was funded by the Ministry of National Science Foundation (ROC) under Contract No. NSC97-2112-M-214-003 and I-Shou University under Contract No. ISU-108-01-04A.

Author contributions

H.T.L. carried out device fabrication and data collection. Y.M.W. carried out the theoretical analysis and wrote the manuscript.

Competing interests

The authors declare no competing interests.

Additional information

Correspondence and requests for materials should be addressed to Y.-M.W.

Reprints and permissions information is available at www.nature.com/reprints.

Publisher's note Springer Nature remains neutral with regard to jurisdictional claims in published maps and institutional affiliations.